



**HAL**  
open science

## Force networks in granular packing

Farhang Radjai, D.E. Wolf, Stéphane Roux, Michel Jean, Jean Jacques  
Moreau

► **To cite this version:**

Farhang Radjai, D.E. Wolf, Stéphane Roux, Michel Jean, Jean Jacques Moreau. Force networks in granular packing. HLRZ-Workshop on Friction, Arching, Contact Dynamics, 1997, Singapour, Singapore. pp.169 - 179. hal-01824807

**HAL Id: hal-01824807**

**<https://hal.science/hal-01824807>**

Submitted on 27 Jun 2018

**HAL** is a multi-disciplinary open access archive for the deposit and dissemination of scientific research documents, whether they are published or not. The documents may come from teaching and research institutions in France or abroad, or from public or private research centers.

L'archive ouverte pluridisciplinaire **HAL**, est destinée au dépôt et à la diffusion de documents scientifiques de niveau recherche, publiés ou non, émanant des établissements d'enseignement et de recherche français ou étrangers, des laboratoires publics ou privés.

in: (Grassberger, P. et Wolf, D., eds.) *Proc. HLRZ-Workshop on Friction, Arching, Contact Dynamics*, World Scientific, Singapore, 1997, pp. 169-179.

## FORCE NETWORKS IN GRANULAR PACKINGS

F. RADJAI, D. WOLF

*HLRZ, KFA-Jülich, 52425 Jülich, Germany*

S. ROUX

*LPMMH, ESPCI, 10 rue Vauquelin, 75231 Paris Cedex 05, France*

M. JEAN

*IMT-LMA, Technopole de Château Gombert, 13451 Marseille, Cedex 20, France*

J. J. MOREAU

*LMGC, Université des Sciences et Techniques, Place Eugène Bataillon, 34095 Montpellier Cedex 05, France*

We used a Contact Dynamics algorithm to investigate some of the statistical properties of the contact network in quasistatically driven assemblies of rigid particles containing from 500 to 4000 particles in two dimensions. We found that the contact network at every stage of deformation is composed of two complementary subnetworks: a “strong” percolating subnetwork of the contacts carrying a force larger than the mean force (containing about 40% of contacts), and a “weak” subnetwork of the contacts carrying a force lower than the mean force. In the strong subnetwork, all contacts are nonsliding and the probability distribution of forces is well fitted by an exponential decay. Almost the whole dissipation takes place inside the weak subnetwork, where the number of forces decays as a power-law. The weak subnetwork contributes only to the mean pressure (about 25%), whereas the strong subnetwork takes over the whole deviatoric load. The strong subnetwork bears the primary anisotropy induced by shear with the same orientation as the stress tensor, but it gives rise to a secondary anisotropy inside the weak subnetwork with an orientation orthogonal to that of the stress tensor.

### 1 Introduction

Photoelastic visualizations provide a direct evidence for the *heterogeneous* distribution of contact forces in dense granular systems (see Fig. 1),<sup>1</sup> with the following qualitative features:

1. Contact-to-contact fluctuations over several orders of magnitude,
2. Correlations on a scale far larger than the particle size,
3. Rapid reorganization during deformation.

Micromechanical modeling of granular materials in the dense regime involves a quantitative characterization of both statistical distributions and spatio-temporal correlations of internal variables on the scale of these heterogeneities.<sup>2</sup> The necessity of considering such a detailed microscopic study has been frequently observed since Coulomb, who introduced the first phenomenological concepts in the field.<sup>3</sup> Recently, a significant effort has been made in this direction through experiments,<sup>4,5,6,7</sup> numerical simulations,<sup>8,9,10,11</sup> and theoretical modeling.<sup>12,13,14,15</sup> This effort is justified regarding the fact that the statistical distributions of internal mechanical variables are quite large.<sup>11</sup> This means that the mean quantities, commonly used to model the quasistatic deformation of granular media, provide only a marginal information.

In this paper, on the basis of numerical results from simulations of a few thousands of particles in two dimensions, we show that the organization of these variables

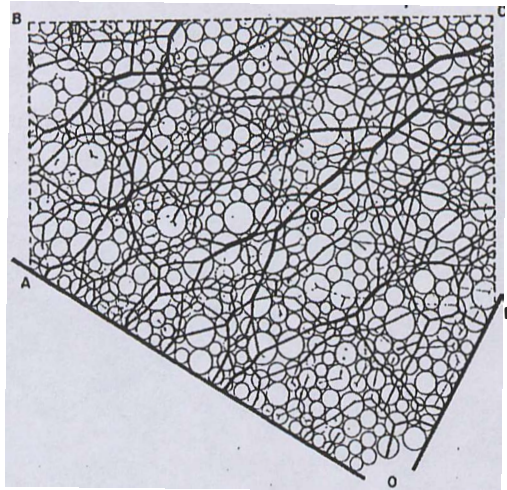


Figure 1: Contact forces in a sheared assembly of disks, visualized using the photoelastic effect, and encoded as widths of intercenter segments [Drescher and de Josselin de Jong, 1972].

has a basic *bimodal* character, which is also reflected in the structure of the stress tensor. We will first briefly introduce the simulation method. Then, we will focus successively on force distributions, stress tensor, induced anisotropy, and dissipation.

## 2 Simulation method

A numerical simulation of a densely-packed system has to tackle a *multicontact* problem. Every collision in such a medium is a multiple collision that cannot be reduced to a set of independent binary collisions since impulsions propagate through the contact network and may even leave the system. In the same way, the frictional resistance to shear is a collective phenomenon involving the mobilization of friction at kinematically correlated contacts. Another basic problem is that the contact laws are strongly *nonlinear*. In the approximation of perfectly rigid particles, the normal force at a contact is not given locally as a function of the relative displacement of two particles, but rather as a result of the global geometrical configuration of the whole system and the boundary conditions. Furthermore, the basic Coulomb's law of friction is *nonsmooth* in the sense that the relation between the relative tangential velocity and the friction force cannot be represented as a mathematical function.

The Contact Dynamics (CD) method, which was used for the investigations reported in this paper, takes these features into account on a mathematical basis derived from Convex Analysis.<sup>16,17</sup> On one hand, the conditions of *perfect rigidity* and *exact Coulombian friction* are implemented with no resort to any regularization. On the other hand, all kinematic constraints are *simultaneously* taken into account, together with the equations of dynamics, in order to determine contact forces and

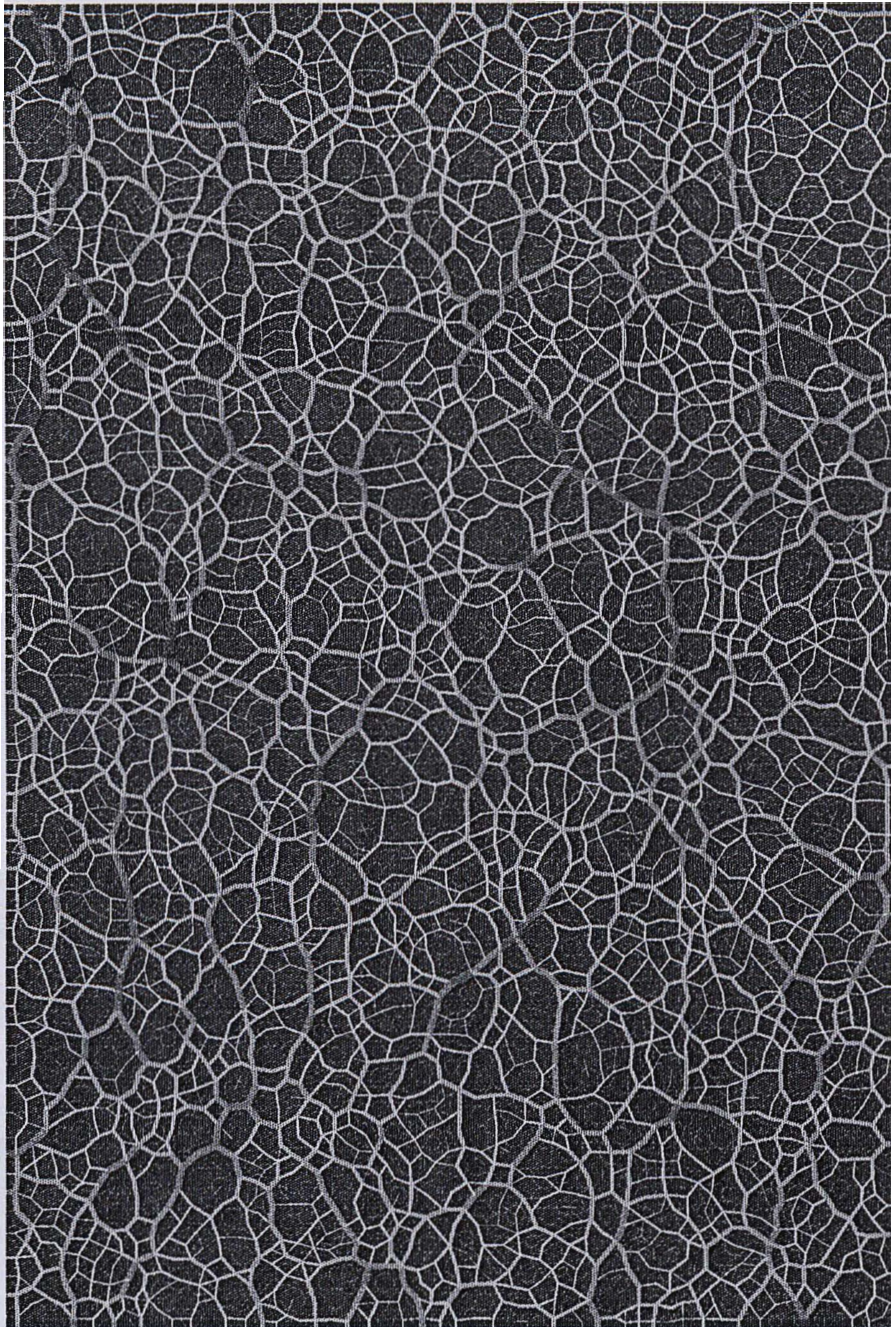


Figure 2: Normal components of the contact forces in sample A (see text) encoded both as the widths of intercenter connecting segments and by the color intensity.

particle velocities in the system. The method is thus able to deal properly with the *nonlocal* character of the momentum transfers in the contact network.

Let us underline here the point that *dynamics* is an essential ingredient of this approach. It is well known that a granular system at static equilibrium is *hyperstatic*, i.e. for given boundary conditions there is a continuous set of possible contact forces. This is due both to the absence of an internal displacement field (because of perfect rigidity) and to the nonsmooth character of the friction law.<sup>18</sup> In the CD method, the force network at static equilibrium is determined through the *dynamic processes* from which it relaxed. In other words, like in real granular systems, the static values of forces are reached asymptotically as the kinematic energy of the system is dissipated in friction and collisions.

### 3 Force distributions

Let us begin with the probability distribution  $P_N$  of normal forces  $N$  independently of contact orientations. Numerical results will be presented here for three samples of 4012, 4025, and 4098 particles, referred to as samples A, B, and C. Particles are contained in a rectangular frame composed of two horizontal and two vertical rigid walls. Sample A is biaxially compressed by allowing the inward motion of a horizontal wall and by applying a confining load on a vertical wall free to move horizontally. Sample B is in relaxation towards static equilibrium under a confining load applied to a free wall. Sample C is in static equilibrium under confining loads. The acceleration of gravity and the particle-wall coefficients of friction are set to zero. The interparticle coefficient of friction is 0.5 in samples A and C, and 0.2 in sample B. In all samples, the particle radii are uniformly distributed between 3.8 and 7.5 mm.

Fig. 2 displays the normal forces in sample A at an advanced stage of deformation. The force network is in very good qualitative agreement with optical images such as the one shown in Fig. 1. Figs. 3(a) and 3(b) display the plot of  $P_N$  on semilog and log-log scales in the three samples. In all cases, independently of the confining load, the normal forces lower than the mean normal force  $\langle N \rangle$  have a power-law distribution, whereas the data for forces larger than  $\langle N \rangle$  are well fitted by an exponential decay:

$$P_N \propto \begin{cases} \left(\frac{N}{\langle N \rangle}\right)^{-\alpha} & N < \langle N \rangle, \\ e^{-\beta(1-N/\langle N \rangle)} & N > \langle N \rangle. \end{cases} \quad (1)$$

Within the statistical precision, the values of exponents  $\alpha$  and  $\beta$  depend only weakly on the mechanical parameters and the preparation conditions of each sample. In static equilibrium or in quasistatic deformation, the value of  $\alpha$  is very close to zero. However, it seems that  $\alpha$  increases with the degree of dynamics inside the system and decreases with the coordination number. Let us also remark that, since the mean value  $\langle N \rangle$  separates the two parts of the distribution,  $\alpha$  and  $\beta$  should be related together by the equation  $\beta^2 = (1 - \alpha)(2 - \alpha)$ , which is approximately satisfied in our simulations.

As far as the distribution  $P_T$  of the absolute values of friction forces  $T$  is concerned, we find a power law decay for forces lower than the mean friction force  $\langle T \rangle$

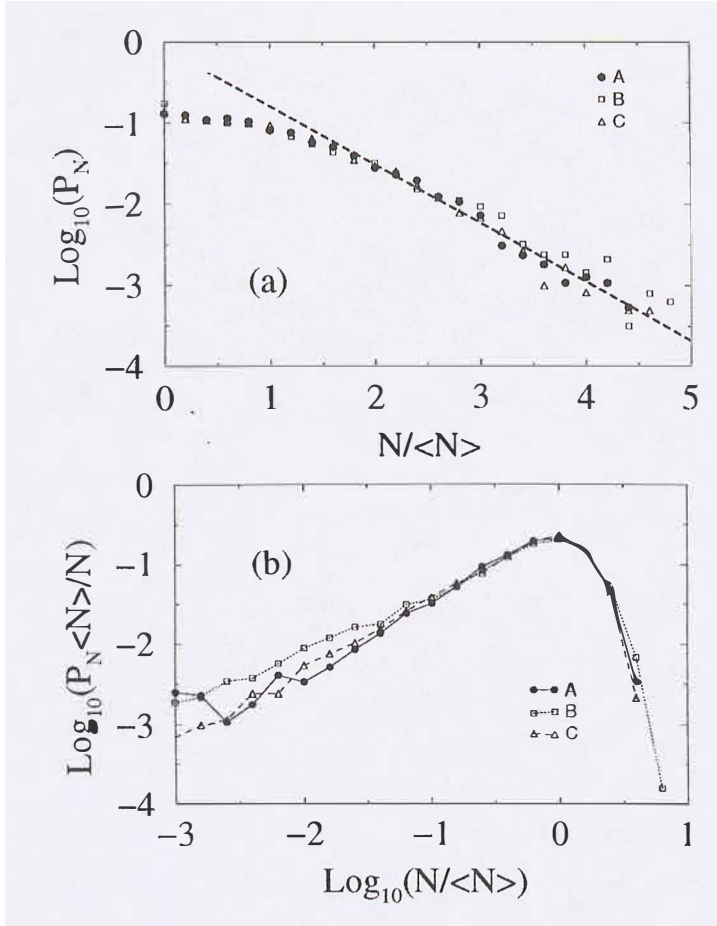


Figure 3: (a) Semilogarithmic, and (b) log-log plots of the probability distribution  $P_N$  of normal forces  $N$ .

and a decreasing exponential function for friction forces higher than  $\langle T \rangle$ , as shown in Figs. 4(a) and 4(b).

$$P_T \propto \begin{cases} \left(\frac{T}{\langle T \rangle}\right)^{-\alpha'} & T < \langle T \rangle, \\ e^{\beta'(1-T/\langle T \rangle)} & T > \langle T \rangle. \end{cases} \quad (2)$$

This distinction between the forces lower than the mean, to which we will refer as “weak” forces, and those larger than the mean, referred to as “strong” forces in the following, has a deep meaning, as we shall see below. Let us only mention here that the exponential distribution of strong forces does not seem to be a finite-size effect. In other words, a simple normalization of the forces with respect to the mean force allows the data to collapse almost on the same curve for samples of 500 to 4000 particles.<sup>11</sup>

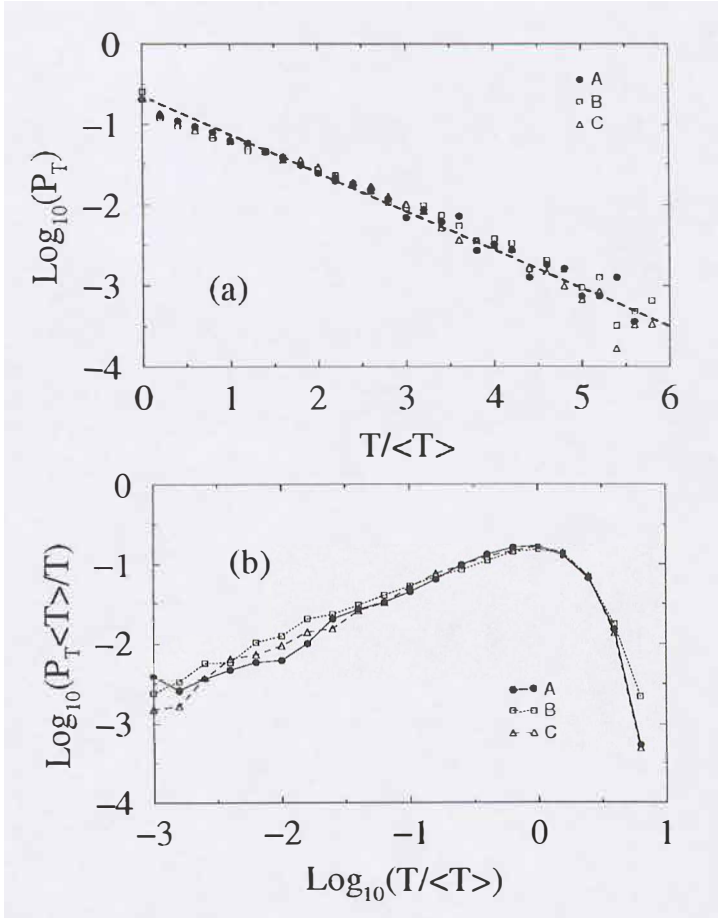


Figure 4: (a) Semilogarithmic, and (b) log-log plots of the probability distribution  $P_T$  of friction forces  $T$ .

The exponential distribution of strong normal forces, has been observed in experiments.<sup>6,7</sup> Weak normal forces and friction forces at individual contacts are technically difficult to measure, and their distributions have not yet been observed experimentally. The power-law decay or the uniform distribution of weak forces, comprising nearly 60% of contacts, indicates that the weak forces are generated through a self-similar branching process from strong forces. In contrast, the strong forces are conditioned by the level of the deviatoric load, which sets in effect a characteristic force different from the mean force. This point will become more clear by the study of the stress tensor.

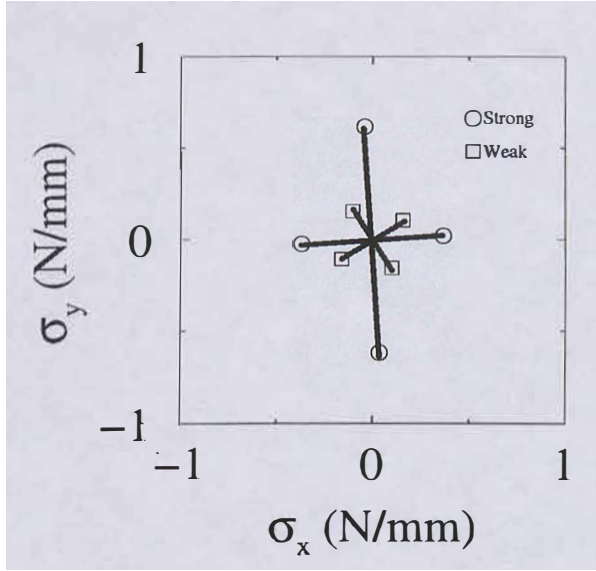


Figure 5: Contributions of weak and strong contacts to the stress tensor in sample A at shear peak.

#### 4 Stress tensor

The stress tensor is the relevant variable in transition to the continuous limit. In contrast to  $P_N$  and  $P_T$ , it involves both the contact forces and the contact orientations according to the following classical formula:<sup>19</sup>

$$\sigma_{ij} = \frac{1}{V(\Omega)} \sum_{c \in \Omega} f_i^c d_j^c, \quad (3)$$

where  $\Omega$  is the region inside the sample for which the stress tensor is calculated with a volume equal to  $V$ ,  $f_i^c$  is the  $i$ -component of the force at the contact  $c$ , and  $d_j^c$  is the  $j$ -component of the intercenter vector  $\mathbf{d}^c$ . This equation allows to separate the contributions of weak and strong forces to the global stress tensor. The weak tensor  $\sigma^w$  and the strong tensor  $\sigma^s$  are given by the above equation when the summation is restricted to only weak contacts and only strong contacts, respectively.

Among our samples, only sample A, due to its uniform stress field, provides enough statistics for the study of the stress tensor. Fig. 5 shows the orientations and the eigenvalues of  $\sigma^w$  and  $\sigma^s$  in sample A at shear peak, i.e. at the maximal value of  $q = \frac{\sigma_1 - \sigma_2}{\sigma_1 + \sigma_2}$ , ( $q = 0.18$ ), where  $\sigma_1$  and  $\sigma_2$  are the principal values of the total stress tensor  $\sigma = \sigma^w + \sigma^s$ . We see that  $\sigma^w$  is almost spherical and contributes no more than 3% to the deviatoric part of the total stress tensor  $\sigma$ , whereas  $\sigma^s$  represents almost the whole deviatoric load, and its major principal axis has the same orientation as that of the imposed deformation.

The isotropic nature of the weak stress tensor indicates that the weak contacts feel the influence of the deviatoric load only as an average over all directions. The

strong contacts directly support the deviatoric load, whose signature appears as a characteristic force in the exponential decay of strong forces.

## 5 Induced anisotropy

We now consider the distribution  $P_\theta$  of contact orientations. The anisotropic nature of  $P_\theta$  has been extensively studied in the past.<sup>20,21,22,9,8</sup> Here, we define two separate distributions  $P_\theta^w$  and  $P_\theta^s$  for weak and strong contacts, respectively. The polar diagrams of these distributions are shown in Fig. 6 for sample A at shear peak. We see that both distributions are anisotropic, although to a lesser extent in the weak subnetwork than in the strong one. The interesting behavior observed here is that the principal direction of  $P_\theta^s$  coincides with that of the stress tensor, whereas the principal direction of  $P_\theta^w$  is *orthogonal*! This again confirms the bimodal nature of the force network, and clearly shows the *complementarity* between the two subnetworks: The strong chains need “lateral” weak forces in order to be stable.

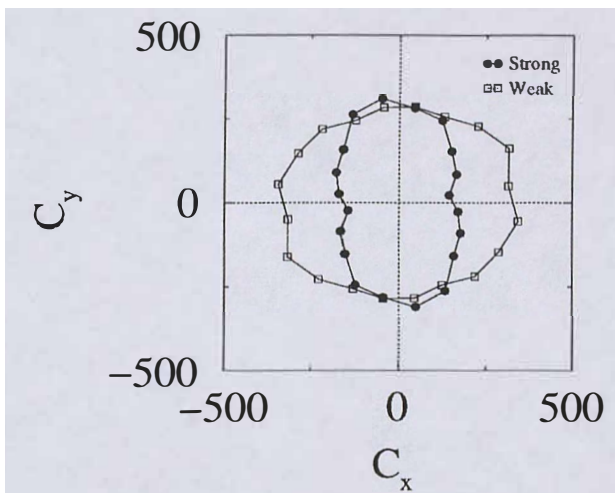


Figure 6: Polar diagram of the distribution of contact orientations in weak and strong subnetworks.

## 6 Dissipation

Particle rotations constitute one of the difficult aspects of the micromechanics of granular materials in quasistatic deformation. The possibility of particles to roll over one another provides a very low-dissipative local mechanism of deformation, so that if each particle could roll over its neighbors, then a dense granular system would essentially behave like a liquid. However, in a quasistatically driven system, the particle rotations are generically *frustrated*, i.e. particles cannot move and rotate without sliding at some contacts in the medium. This gives rise to long-range correlations with patterns that have been partially studied in the case of

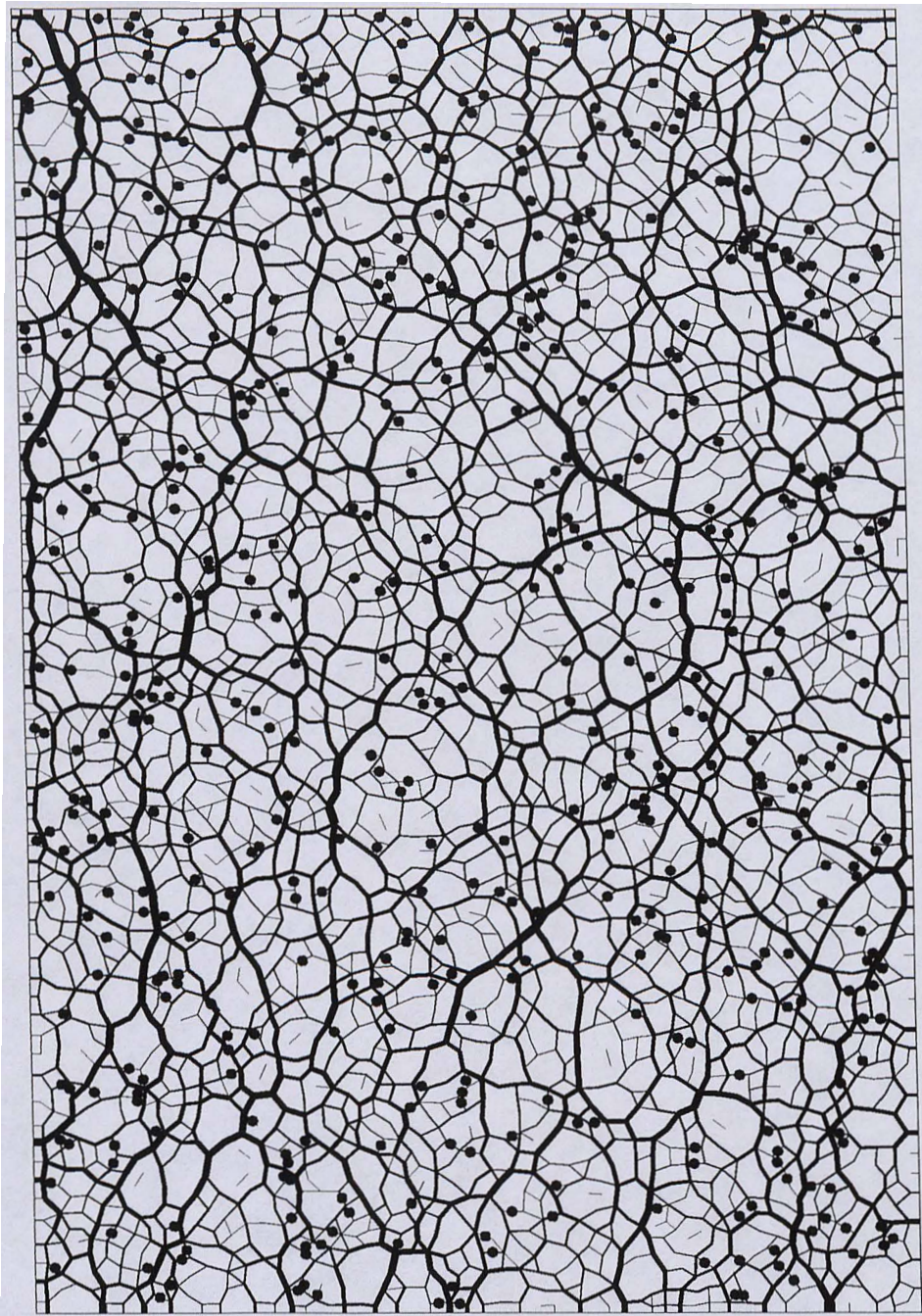


Figure 7: Network of normal forces in sample A. Forces are encoded as the widths of intercenter segments. Weak and strong subnetworks are shown with two different colors. The filled circles show the positions of sliding contacts.

regular packings.<sup>18,23</sup> The question we would like to raise here is how the positions of *sliding* contacts in the contact network are correlated with the contact forces?

The distinction between weak and strong subnetworks again provides a simple key to the problem. In Fig. 7, we have shown the two subnetworks with different colors and the positions of the sliding contacts. Only 8% of contacts are sliding, and a rapid inspection shows that almost all of them are on the weak subnetwork. In other words, all strong contacts are nonsliding and all the dissipation takes within the weak subnetwork. This remarkably simple behavior of the sliding contacts with respect to the force subnetworks shows the *dynamic* nature of the bimodal distribution of forces. The strong subnetwork is *completely* unstable since all its contacts are nonsliding. As a result, it tends to buckle under the action of the external deviatoric load, giving rise to an orthogonal anisotropy and sliding contacts in the weak subnetwork.

## 7 Conclusion

The observations briefly presented above provide a consistent picture of the internal mechanical state of a granular packing in quasistatic deformation, at least in two dimensions. The contact network is composed of two complementary subnetworks:

1. A “load-bearing” percolating subnetwork composed of strong contacts;
2. A “dissipative” subnetwork composed of weak contacts.

The strong subnetwork supports the whole deviatoric load applied on the system, although it contains only nonsliding (nondissipative) contacts. The whole dissipation takes place inside the weak subnetwork. This implies that the scale of heterogeneity of a granular system due to sliding and nonsliding states of contacts is the same as that of the strong subnetwork. From the point of view of the stress tensor, the weak subnetwork behaves like an interstitial liquid, whereas the strong subnetwork has a solid-like behavior since it takes over the whole deviatoric load and thus the stability of the system. From the point of view of the fabric tensor (or contact orientations), the strong subnetwork bears the *primary* anisotropy induced by shear, but it gives rise to a *secondary* orthogonal anisotropy inside the weak subnetwork.

This two-phase behavior of the force network opens new perspectives both for microscopic and macroscopic modeling of granular materials in quasistatic deformation. Let us, however, recall that the analysis presented above concerns a two-dimensional system. It is not obvious that it works in the same manner in three-dimensional systems. In a two-dimensional packing, two oppositely-oriented arches of strong contacts may surround a region composed of weak contacts alone. This topological feature suggests a mechanism to explain the two-phase behavior in two-dimensional systems. Nevertheless, there are reasons to believe that there is a more general mechanism relevant to three-dimensional systems too.

## Acknowledgements

It is a pleasure to acknowledge many fruitful discussions with U. Bastolla and L. Brendel.

## References

1. P. Dantu in *Proceedings of the 4th International Conference on Soil Mechanics and Foundations Engineering* (Butterworths Scientific Publications, London, 1957).
2. H. M. Jaeger, S.R. Nagel, and R. P. Behringer, *Rev. Mod. Phys.* **68**, (1996).
3. C. de Coulomb, *Mémoires de mathématiques et de physique* (Imprimerie Royale, Paris, 1773).
4. T. Travers, D. Bideau, A. Gervois, and J. C. Messenger, *J. Phys. A* **19**, L1033 (1986).
5. A. Drescher and G. de Josselin de Jong, *J. Mech. Phys. Solids* **20**, 337 (1972).
6. C.-h. Liu, S. R. Nagel, D. A. Schecter, S. N. Coppersmith, S. Majumdar, O. Narayan, and T. A. Witten, *Science* **269**, 513 (1995).
7. B. Miller, C. O'Hern, and R. P. Behringer, *Phys. Rev. Lett.* **77**, 3110 (1996).
8. L. Rothenburg and R. J. Bathurst, *Géotechnique* **39**, 601 (1989).
9. B. Cambou and F. Sidoroff, *J. Mech. Th. Appl.* **4**, 223 (1985).
10. K. Bagi, in *Powders and Grains 93*, ed. C. Thornton (Balkema, Rotterdam, 1993).
11. F. Radjai, M. Jean, J. J. Moreau, and S. Roux, *Phys. Rev. Lett.* **77**, 274 (1996).
12. S. N. Coppersmith, C.-h. Liu, S. Majumdar, O. Narayan, and T. A. Witten, preprint.
13. S. F. Edwards and C. C. Mounfield, *Physica A* **226**, 1 (1996).
14. J. P. Bouchaud, M. E. Cates, and P. Claudin, *J. Physique* **5**, 639 (1995).
15. S. Ouaguenouni and J. N. Roux, preprint; J. Hemmingsson, H. J. Herrmann, and S. Roux, preprint; E. Clément, C. Eloy, J. Rajchenbach, and J. Duran, preprint; S. Luding, preprint.
16. J. J. Moreau, *Eur. J. Mech. A/Solids* **13**, 93 (1994).
17. M. Jean in *Mechanics of Geometrical Interfaces*, ed. A. P. S. Selvadurai and M. J. Boulon (Elsevier, Amsterdam, 1995).
18. F. Radjai, L. Brendel, and S. Roux, *Phys. Rev. E* **54**, 861 (1996).
19. J. Christoffersen, M. M. Mehrabadi and S. Nemat-Nasser, *J. Appl. Mech.* **48**, 339 (1981).
20. J. Biarez and K. Wiendick, *C. R. Acad. Sci.* **256**, 1217 (1963).
21. M. Satake in *Theoretical and Applied Mechanics* (Tokyo University Press, Tokyo, 1978).
22. M. Oda and J. Koshini, *Soils and Foundations* **14**, 25 (1974).
23. F. Radjai and S. Roux, *Phys. Rev. E* **51**, 6177 (1995).